

# Efficiency tests for estimating the gas and stellar population parameters in Type 2 objects

Bon, N.<sup>a,b</sup>, Popović L. Č.<sup>a</sup>, & Bon, E.<sup>a</sup>

<sup>a</sup>*Astronomical Observatory, Belgrade, 11060 Serbia*

<sup>b</sup>*Observatoire de Lyon, 9 avenue Charles André, Saint-Genis Laval cedex, F-69561, France ;  
CNRS, UMR 5574*

---

## Abstract

We investigated the efficiency of estimating characteristics of stellar populations (SP) and Active Galactic Nuclei (AGN) emission using ULYSS code. To analyse simultaneously AGN and SP components in the integrated spectrum of Type 2 active galaxies, we modelled the featureless continuum (FC) and emission lines, and we used PEGASE.HR stellar population models provided by ULYSS. In order to validate the method, we simulated over 7000 integrated spectra of Seyfert 2 galaxies. Spectra were generated using different characteristics of the featureless AGN continuum, signal-to-noise ratio (SNR), spectral ranges, properties of emission lines and single stellar population (SSP) model whose initial mass function (IMF) and abundance pattern is similar to the solar neighbourhood. Simulated spectra were fitted with ULYSS to evaluate the ability of the method to extract SP and AGN properties. We found that the analysis with ULYSS can efficiently restore the characteristics of SP in spectra of Seyfert 2 AGNs, where signal-to-noise ratio is higher than 20, and where SP contributes with more than 10% to the total flux. Degeneracies between AGN and SP parameters increase with increasing the AGN continuum fraction, which points out the importance of simultaneous fitting of the FC and SP contributions.

*Keywords:* techniques: spectroscopic, methods: data analysis, galaxies: active, galaxies: stellar content

---

---

*Email address:* nbon@aob.bg.ac.rs (Bon, N.)

## 1. INTRODUCTION

Spectra of Seyfert 2 galaxies can consist of two main components: (1) a stellar component characterized by absorption lines from stellar atmospheres and (2) an Active Galactic Nucleus (AGN) component formed of emission lines and a featureless continuum (FC). In the standard AGN model the UV/optical continuum is produced by non-thermal processes, following a power-law in the form  $f_\lambda \sim \lambda^\alpha$  with a typical value of  $\alpha$  in the range  $\alpha = [-1.5, 2]$  (e.g. [Kinney et al., 1991](#); [Boroson & Green, 1992](#); [Winkler et al., 1992](#)). In the frame of the AGN unified model (see [Antonucci, 1993](#)), a direct view of the continuum source is blocked by a dense molecular torus in the case of the Seyfert 2 objects. The observed featureless continuum is believed to be a nuclear starlight, scattered by free electrons and dust. However, hot, young stars also produce a featureless continuum that attenuates the absorption lines of the older stellar population ([Nelson & Whittle, 2000](#)). It was suggested in a number of studies ([Cid Fernandes & Terlevich, 1995](#); [Colina et al., 1997](#); [Schmitt et al., 1999](#)) that the UV continua in Sy 2 galaxies may have a considerable contribution from the nuclear star formation. Therefore, any reliable measurement of the emission-line spectrum of galactic nuclei has to properly account for the influence of starlight. On the other hand, to reliably derive the stellar population properties of these Sy 2 host galaxies, the contribution from the AGN continuum and emission lines must be properly considered (see e.g. [Goudfrooij & Emsellem, 1996](#); [Moore et al., 2002](#); [Sarzi et al., 2006](#)). Namely, stellar absorption spectra are contaminated by emission lines. For example, wavelength bend of Mg I lines at  $\lambda\lambda 5167, 5175, 5184$ , which are traditionally used for stellar population studies are blended by strong emission [NI] and [FeVII] lines. Furthermore, absorption lines are diluted in some degree by the nuclear continuum.

A typical approach to investigate gas properties in the centre of an AGN is to decompose the spectrum into different components in order to remove starlight from an integrated spectrum. There are a number of methods for removing the starlight contribution. The most frequently used one is the method of the template subtraction. A number of approaches have been adopted to construct the template, as e.g.: (i) the spectrum of an off-nuclear position within the same galaxy (e.g. [Storchi Bergman et al., 1993](#)), (ii) the spectrum of a different similar galaxy without emission lines (e.g. [Ho et al., 1993](#)), (iii) a mean spectrum derived from a principal-component analysis of a large set of galaxies ([Hao et al., 2005](#); [Vanden Berk et al., 2006](#)) and (iv) a model spectrum constructed from population synthesis techniques (e.g. [Keel, 1983](#); [Bonatto et al., 1989](#); [Sarzi et al., 2005](#)).

In order to minimize degeneracies between spectrum components, it is better

to avoid the subtraction of the stellar population (SP) from the total spectrum before the analysis of the AGN emission, and to fit simultaneously all constituents that contribute to the total spectrum. One of the techniques for the analysis of an unresolved component from stellar populations in an integrated spectrum is the spectral synthesis technique, which consists in the decomposition of an observed spectrum in terms of single stellar populations (SSPs) of various ages and metallicities, producing as an output the star formation and chemical enrichment histories of a galaxy, together with its velocity dispersion (e.g. [Cid Fernandes et al., 2005](#); [Chilingarian et al., 2007](#); [Koleva et al., 2009](#); [MacArthur et al., 2009](#); [Cid Fernandes & González Delgado, 2010](#)). This is achieved by a full spectrum fitting including the continuum shape and absorption features.

One of the most popular techniques for the spectral decomposition of AGN host galaxies is GANDALF, developed by Marc Sarzi ([Sarzi et al., 2006](#)). At the same time GANDALF fits velocity broadened SSP models and Gaussians representing the emission lines. It performs the full spectral fitting of an observed spectrum with a set of SSP models, determining the line of sight velocity distribution (LOSVD), the best-fit stellar population model and kinematical characteristics of the gas. The GANDALF code, however, does not consider the continuum radiation from the central source, which, instead, is accounted for by the method proposed in this paper.

Here we present and test the method for simultaneous analysis of gas and stellar kinematics, star formation history and continuum radiation in the spectra of Seyfert 2 galaxies. For this purpose we introduce the power law continuum and emission lines in the model of ULySS ([Koleva et al., 2009](#)). The importance of introducing the featureless AGN continuum in the analysis was explained by [Moultaka \(2005\)](#). Namely, [Moultaka \(2005\)](#) showed that the SP composition is highly affected by the presence of an additive continuum, if this continuum is not modelled in the synthesis.

The goal of our tests is not to model the stellar populations of the host galaxies, which can be complicated by the presence of star forming regions (see e.g. [Smirnova et al., 2007](#); [Popović et al., 2009](#)). On the contrary, we study under which conditions an aged stellar population can still be recovered in presence of an overlapped AGN continuum.

The paper is organized as follows: In Section 2 and 3 we describe the method; in Section 4 we test its validity and limitations, by simulating and fitting several thousands of spectra; in Section 5 we give the discussion of obtained results and finally in Section 6 we outline our conclusions.

## 2. The method for stellar population fitting in AGN spectra

In order to analyse AGN spectra, we adjusted ULySS (Koleva et al., 2009) full spectrum fitting package. The code was adapted to analyse simultaneously all components of the integrated light from an active galaxy.

ULySS<sup>1</sup> generated model represents bounded linear combination of non-linear components convolved with a broadening function and multiplied by a smooth free continuum, with a possibility to use a polynomial additive term. The model is generated at the same resolution and with the same sampling as the observation and the fit is performed in the pixel space. The fitting method consists in minimizing the  $\chi^2$  between an observed spectrum and a model. It performs the Levenberg-Marquart minimization (Marquart, 1963). The code is written in IDL/GDL starting from PPXF<sup>2</sup>(Cappellari & Emsellem, 2004) and uses the MPFIT<sup>3</sup> procedure.

Single stellar population (SSP)<sup>4</sup> models used by ULySS are spline interpolated over an age-metallicity grid of models. ULySS can use any library of stellar spectra. Some models for stellar population spectra are provided by ULySS web-page, such as grid of PEGASE.HR SSPs, computed with the Elodie.3.1 library and a Salpeter IMF (Le Borgne et al., 2004) or the grid of Vazdekis models computed with the Miles library and Salpeter IMF (version 9, published in Vazdekis et al. (2010)). Therefore, by fitting a spectrum with ULySS, we reconstruct the SSP-equivalent age and metallicity.

ULySS has been used to study stellar populations (Bouchard et al., 2010; Koleva et al., 2011, 2013) and determine atmospheric parameters of stars (Wu et al., 2011).

Following Barth et al. (2002) we defined a model  $M(x)$  of an integrated AGN spectrum, consisting of a stellar template spectrum  $T(x)$  convolved with a line-of-sight velocity broadening function  $G(x)$ , a model for the AGN continuum  $C(x)$ , and a sum of Gaussian/Gauss-Hermit functions  $S(x)$ , that represent AGN emission lines:

$$M(x) = P(x)\{[w_0T(x) \otimes G(x)] + w_1C(x) + \sum_{i=2}^n w_iS_i(x)\}, \quad (1)$$

were  $P(x)$  is a multiplicative polynomial.

---

<sup>1</sup>ULySS is available at: <http://ulyss.univ-lyon1.fr/>

<sup>2</sup><http://www-astro.physics.ox.ac.uk/mxc/idl/> The current version of ULySS does not depend on the ppxf.

<sup>3</sup>Markwardt, <http://www.physics.wisc.edu/craigm/idl/fitting.html>

<sup>4</sup>SSP is population with single age and metallicity.

For simplicity, we assumed a Gaussian velocity broadening function  $G(x)$ , but it is possible to use also Gauss-Hermite polynomials (GH) of the 3rd and 4th order accounting for deviations of the galaxy’s LOSVD from Gaussian. The 3rd order of the GH polynomial is responsible for the asymmetry in the line profile (h3), while its 4th order stands for the symmetric deviation from a Gaussian (narrower for positive or wider for negative h4, respectively; see e.g. [Rix & White \(1992\)](#); [van der Marel \(1994\)](#)).

The mismatch between the shapes of galaxy and stellar spectra occurs because spectra of distant galaxies are obtained with different gratings and detectors from the stellar template spectra that are used in the spectral libraries. Therefore, the spectra of the stars and the distant galaxies may have different continuum shapes due to the multiplicative instrumental response function (see e.g. [Eriksson et al., 2006](#)). So, we introduced a multiplicative polynomial  $P(x)$ , into the fit to remove overall shape differences between the observed stellar and galactic spectra. The introduction of this polynomial in the fit ensures that results are insensitive to the normalization, the flux calibration of a galaxy and stellar template spectra, but also to the Galactic extinction ([Koleva et al., 2008](#)). The continuum of the stellar template and galaxy spectra is normalized during the continuum matching process. This normalization becomes a part of the  $\chi^2$  minimization, and consequently the effects of the continuum normalization on derived velocity dispersions are, by definition, minimized ([Kelson et al., 2000](#)). The multiplicative polynomial represents a linear combination of Legendre polynomials.

The contribution of the components to the total flux can be calculated from their weights ( $w_i$ ) which are determined at each Levenberg-Marquart iteration using a bounding value least-square method ([Lawson & Hanson, 1995](#)).

In our test we used PEGASE.HR SSP grid as it is provided by ULySS, in the wavelength range  $\lambda\lambda = [3900, 6800] \text{ \AA}$ .

### 3. Components of the model

Beside the stellar population, we used featureless continuum and emission lines in the model of integrated spectra of Seyfert 2 galaxies.

#### 3.1. Featureless continuum

In the original version of ULySS, the optional additive continuum  $C(x)$  is represented by Legendre additive polynomial. Here we used  $C(x)$  as a non-stellar

component, represented by a power law  $f_\lambda \sim \lambda^\alpha$ , where  $\alpha$  represents the free parameter in the fit, together with the weight of this component.

The additive continuum was added to the stellar base to represent the contribution of an AGN featureless continuum (FC), a traditional ingredient in the spectral modelling of Seyfert galaxies since (Koski, 1978). The spectral index  $\alpha$  depends on the continuum slope, thus in different spectral domains it has different values. For the optical domain, that we analysed, the expected value for the spectral index is usually in the interval between -1.5 and 2 (e.g. Kinney et al., 1991; Boroson & Green, 1992; Winkler et al., 1992). In the frame of the unified model (e.g. Antonucci, 1993), in Seyfert 2s this FC, if present, must be scattered radiation from the hidden type 1 Seyfert nucleus. Nevertheless, one must keep in mind that young starbursts can easily look like an AGN continuum in optical spectra, that presents a common problem faced in spectral synthesis of Seyfert 2s (Cid Fernandes & Terlevich, 1995; Storchi Bergman et al., 2000).

The routine for the featureless continuum definition, that we use is adequate to the power function on the ULySS web page, tutorial 4.

### 3.2. Emission lines

When we construct a model of narrow emission lines such as those that can be found in Seyfert 2 galaxies, we made a routine to define each emission line component separately as a Gaussian or Gauss-Hermit function. Figure 1 gives the possibility for a visual comparison between the real spectrum of Seyfert 2 galaxy and the simulated one.

Dealing with separate emission line models, ULySS allows to constrain the relations between parameters of the different lines. Theoretical calculations (Rosa, 1985; Galavís et al., 1997) and measurements of the line characteristics in the case of ionized nebulae and AGN (see e.g. Acker et al., 1989; Dimitrijević et al., 2007) indicate the relationship between the flux of certain emission lines, as for example, the constant flux ratio of [OIII] 4959, 5007 Å or [NII] 6548, 6583 lines. Besides, if a group of emission lines arises in the same region, one can expect the same widths and shifts of narrow lines. Taking all of this into account, we set constraints of the line properties during the fit. To constrain emission line parameters we used TIED parameter in PARINFO structure in MPFIT<sup>5</sup>. Tied parameters are considered to be fixed, and therefore no errors are computed for them.

---

<sup>5</sup>PARINFO is an array of structures, one for each parameter, used by MPFIT for simple boundary constraints which can be imposed on parameter values. One of the entries in the PARINFO structure is TIED which can be used to tie one parameter value to other parameter values.

Routine that we use for the emission line model construction (named `uly_Gauss`) is based on the Craig B. Markwardt's routine `gauss1.pro` that could be found at: <http://cow.physics.wisc.edu/~craigm/idl/down/gauss1.pro>.

Similar routine that defines emission lines is provided by ULYSS package (`uly_line.pro`), but we did not test this routine, since our project started from NBurst (Chilingarian et al., 2007) before the publication of ULYSS.

#### 4. Simulations

Once we fit an AGN spectrum with the composite model, we are able to analyse the kinematics of the stellar component and the connection between the gas and stellar motion in a galaxy, as well as the age and metallicity of the stellar population.

In order to test the method, first we performed numerical simulations. The aims of the simulations are: (i) to evaluate the ability of our method to disassociate the stellar population and the pure AGN spectrum from the composite AGN + SP spectrum, which was simulated using different fractions of the featureless continuum, and (ii) to verify the dependencies between the different FC contribution and characteristics of the SP spectra.

To test the accuracy of the method, we simulated line-of-sight integrated spectra of low luminosity AGNs. We assumed that the spectrum is composed by the featureless continuum, emission lines and underlying stellar population (SP) from the host galaxy. We made a grid of 7200 spectra with the PEGASE.HR SSP model whose initial mass function and abundance pattern is similar to the solar neighbourhood (hereafter Solar-like), combined with different fractions and slopes of featureless continuum, different intensities and widths of emission lines, various spectral ranges, SNR and degrees of Legendre multiplicative polynomial. In more details, simulated spectra were made with (i) AGN power-law continuum fractions in the range 10% to 90% to the total continuum (measured at 5100 Å) and spectral indices  $\alpha = -1.5, -0.5, 0.5, 1.5, 2$  (ii) single stellar population spectra produced with PEGASE.HR code with Solar-like characteristics (age=5 Gyr and  $[\text{Fe}/\text{H}] = 0$  dex) and (iii) emission lines. We convolved the SSP spectrum with the Gaussian profile having width (sigma) of 100 km/s in order to mimic the realistic SP velocity dispersion for low luminosity AGNs. We simulated spectra in three spectral ranges: (4000-6700) Å, (4000-5600) Å and (4200-5600) Å, and with 10 signal-to-noise ratios (from 5 to 50). SNR defines mean signal-to-noise ratio of the analysed spectrum. According to this parameter, the program generates a constant error spectrum and add it to the simulated spectrum.

Depending on the spectral range, we simulated emission lines (H $\delta$ , H $\gamma$ , HeII 4689 Å, H $\beta$ , [OIII] 4959, 5007 Å lines, [NII] 6548, 6583 Å and H $\alpha$ ). We linked widths of emission lines as

$$\sigma_{\text{line1}}/\lambda_{\text{line1}} = \sigma_{\text{line2}}/\lambda_{\text{line2}}, \quad (2)$$

where  $\sigma$  and  $\lambda$  are widths and wavelength of corresponding line, respectively. All emission lines shifts were fixed to the same value. Besides, we linked intensities of the [OIII] lines ( $I([\text{OIII}]\lambda 5007 \text{ \AA}) = 3 \times I([\text{OIII}]4959 \text{ \AA})$ ) ( [Dimitrijević et al., 2007](#)), as well as intensities of the [NII] lines ( $I([\text{N II}]6583 \text{ \AA}) = 3 \times I([\text{N II}]6548 \text{ \AA})$ ).

Finally, varying characteristics of the line, we created 25 different [OIII]4959 Å line profiles, using five different intensities and five widths (with FWHM from 200 km s<sup>-1</sup> up to 2000 km s<sup>-1</sup>). Intensities of all the other lines in the model were linked in some ratio with the intensity of [OIII]4959 Å line, while their widths and shift are linked with the [OIII]4959 Å line, as it is described in the previous paragraph.

We made a test to analyse the dependences between the SSP properties and the degree of the multiplicative polynomial (md). We used 50 degrees of the polynomial (from 1 to 50), and we found that in the case when the SP is contributing with more than 75% to the total spectrum and when the SNR is higher than 20, the restored SP properties do not depend much on the degree of the polynomial and the result is stable for the degree of the polynomial higher than 15. Interesting result is obtained for the SP age and metallicity. Namely, even though the restored SP metallicities are very close to the expected one for any md, for all md < 15 they are underestimated, and for all md > 15 they are overestimated. The result for the SP age is opposite. The restored SP ages are overestimated for md < 15, and underestimated for md > 15. Since it is shown in [Koleva et al. \(2008\)](#) that the high order terms of the multiplicative polynomial (md > 50) are well decoupled from all the kinematical and population parameters, the users are highly recommended to use the lowest md that ensures accurate result. From these reasons we used md=15.

To evaluate the ability of the method to restore characteristics of the gas and stars in the nucleus and in the host galaxy, we fitted the simulated spectra with the described models of integrated AGN spectra. We use `uly_ssp.pro`, `uly_power.pro` and `uly_gauss.pro` routines, to define the fitting model. Therefore, we used a series of components, since each emission line corresponds to the separate component in the fit.

In order to analyse the parametric space and dependencies between parameters,



we performed Monte-Carlo simulations and we made  $\chi^2$  maps to find the position of the global minima and possible local minima.

## 5. Results of simulations

To illustrate the goodness of the best fit, and its dependencies on SNR and FC contribution, we show in Figures 2-5 the analysis of simulated spectra with the integrated AGN model. Figure 2 represents the fit of simulated spectra with 10% of FC contribution and SNR=20. Panels (a) and (b) show the total analysed wavelength range, where one can notice that emission lines are fitted very well, i.e. that residuals from prominent emission lines are on the noise level. For better inspection of the absorption line fit, panel (c) expands a small wavelength region, around Mg I b  $\lambda\lambda$  5167, 5173, 5184 triplet. Figure 3 shows the best fit for the case with 70% of the FC contribution to the spectrum and SNR=20. We can notice on figures that residuals are around 3% of the absorption signal. However, the visual inspection was not sufficient for evaluation of the dependencies between restored parameters and the FC contribution.

Figures 4 and 5 illustrate the differences between the best fits of spectra with SNR=5 and SNR=35, respectively. In both cases the contribution of the feature-less continuum is 50%. Residuals from the fit of the spectra with SNR=5 show that the output is not reliable.

Figure 6 represents the restored SSP ages in a response to the FC contribution to the total spectrum (10%-90%) in the cases of SNR=40 (top panel) and SNR=20 (bottom panel). In both cases the method is able to restore the SP age, but if the SP contributes with less than  $\sim 10\%$  to the total spectrum, the uncertainty of the obtained parameters is much higher as reflected in the much larger size of the error bars. The relationship between other SP parameters and FC contribution can be analysed from Tables 1 and 2. These tables list obtained results from the single best fits in the cases of the different AGN continuum contributions to the total spectrum (10%-90%), and for two different signal-to-noise ratios (SNR=20 in Table 1 and SNR=40 in Table 2). Simulated spectra were obtained for spectral index=1.5,  $I([\text{OIII}]4959)=1$  and  $\text{FWHM}([\text{OIII}]4959)=600 \text{ km s}^{-1}$ . The analysed spectral range was 4000-5600 Å. Our method failed to restore kinematic properties of the stellar population (both the velocity dispersion and mean stellar velocity) if the FC contribution is higher than 90%. According to the inspected results, we can conclude that the adjusted ULySS provides reliable results for the stellar population age, metallicity and kinematics if SP contributes more than  $\sim 10\%$  to

the integrated AGN spectrum.

Figure 7 represents the response of the FC continuum contribution and SSP age to the SNR variability. One can notice that the method restores the FC contribution with high precision for any of tested noise level. On the other hand, in the case of low SNR ( $< 20$ ), the restored SP age is not reliable. In Table 3 we give restored values for different signal-to-noise ratios (SNR from 5 to 50). As it can be seen from Table 3 the SP metallicity is well restored for SNR higher than 10. For lower SNR the code is not able to restore the metallicity. Kinematics of the SP, emission line characteristics and featureless continuum characteristics are not that much sensitive to the noise level.

Tables 4-6 show that different spectral ranges do not affect the sensitivity of the fitting method, as it was expected.

We performed Monte Carlo (MC) simulations to visualize biases, errors and degeneracies between parameters, for the case when the SSP equivalent age is 5 Gyr, SSP equivalent metallicity is  $[\text{Fe}/\text{H}]=0$  and when the featureless continuum fraction is 25% and 50%. MC simulations produce an array of solutions which can be exploited to measure the dispersion of the values of the parameters and allow us to view the correlations. Figure 8 illustrates the dependencies between the AGN featureless continuum contribution and (a) mean stellar population age, (b) mean stellar population metallicity ( $[\text{Fe}/\text{H}]$ ). One can notice that the determination of both SP characteristics depends on the FC contribution. Moreover, the dependences are increasing with decreasing of the stellar population contribution to the total continuum. Obtained degeneracies are expected because of the influence of the emission lines and AGN continuum on the stellar population spectrum. For example, SP age is mostly affected by the  $H\beta$  line, so broad emission  $H\beta$  line masks the absorption one and therefore could affect the restored parameter. Besides, FC dilutes the absorption lines such as G-band and Mg I, that affects the SP metallicity.

When we analysed the dependencies between the FC fraction and SSP age, for the case of 50% of the FC contribution to the spectrum (Fig. 8), we noticed a small void at the expected age (5 Gyr). We obtained similar void even for much higher number of MC simulations. For the moment, we do not know what caused the void, but we note that 5 Gyr is still the mean value of the distribution of the solutions.

## 6. Discussions and conclusions

Inspections of the obtained results showed in which conditions our fitting procedure is giving highly accurate results, for both kinematical and physical properties of stellar and gas component of an integrated AGN spectrum. The result depends mainly on the AGN continuum contribution to the total spectrum and on the signal-to-noise ratio.

Detailed inspection of the fit output gave parameters ranges where we can expect to obtain correct results for both the gas and stellar component in the spectrum, and also gave some limitations that one has to have in mind while using this method. We concluded that the parameters of the gas and stars in the galactic spectrum can be well restored if the spectra have  $\text{SNR} > 20$  and if the stellar population fraction is higher than 10%. In the cases of a high noise, the restored value of measurement is close to the expected one, but the error bars increase with the growth of the noise. The accuracy of the fit does not depend on the wavelengths range. Since the fit depends on the initial values of parameters, it is very important to analyse the parametric space before fitting. Emission lines have to be fitted very well in order to estimate correctly the kinematical properties of the stellar population, so one can conclude that the fit of stellar population can not affect the fit of emission lines, but the fit of emission lines can lead to the misfit of the SP. For a good fit it is very important not to misfit some prominent absorption lines, such as Mg I b  $\lambda\lambda$  5167, 5173, 5184 triplet or G band. The results are almost insensitive to the degree of multiplicative polynomial, if the SNR is higher than 20. For lower values of the S/N level, the fit is better for higher values of  $md$  ( $md \gtrsim 15$ ).

Monte-Carlo simulations revealed that the degeneracies between AGN and SP parameters increase with increasing the AGN continuum fraction. This shows that AGN continuum and SP spectra should be fitted at the same time.

The test of the method leads us to conclude that characteristics of the gas and stars in the galaxy can be efficiently restored in a wide range of the parameters. The tested method is mainly limited with the stellar population used in the model. The Solar like SSP that we used in this work can mimic spectra of Seyfert 2 galaxies, when the observed spectra is emitted from the disk, or from approximately the first kpc of the galaxies. We also tested the models for stellar populations at ages of 1, 2 and 4 Gyr, and we did not find any remarkable differences with presented results. We note that in the case of using very young stellar population in the model, the parametric space could be affected in a different way. Yet, an SSP is not a realistic spectrum, since real spectra would be more accurately represented by linear combinations of SSPs. Therefore, a test with composite stellar popula-

tion models would be more appropriate and we are currently working on it.

## 7. Acknowledgements

This research is part of the projects 176001 "Astrophysical spectroscopy of extragalactic objects" and 176003 "Gravitation and the large scale structure of the Universe" supported by the Ministry of Education and Science of the Republic of Serbia.

We would like to thank Philippe Prugniel and Antoine Bouchard for all the help. Also, we thank to referees for very constructive comments that helped to improve the manuscript.

## References

- Acker, A., Köppen, J., Samland, M., Stenholm, B., An estimation study of planetary nebulae in the galactic bulge. I - Spectrophotometric data, *A&AS*, 58, 44-46, 1989.
- Antonucci R. R. J., Unified models for active galactic nuclei and quasars, *ARA&A*, 31, 473-521, 1993.
- Barth, A. J., Ho, L. C., Sargent, W. L. A., Study of the Direct Fitting Method for Measurement of Galaxy Velocity Dispersions, *AJ*, 124, 2607-2614, 2002.
- Bonato, C., Bica, E., Alloin, D., The stellar-free emission component in galactic nuclei - At low-levels, evidence for shock ionization, *A&A*, 226, 23-44, 1989.
- Boroson, T. A., & Green R. F. , The emission-line properties of low-redshift quasi-stellar objects, *ApJS*, 80, 109-135, 1992.
- Bouchard, A., Prugniel, P., Koleva, M., Sharina, M., Stellar population and kinematics of NGC 404, *A&A*, 513, 54-62, 2010.
- Cappellari, M. & Emsellem, E., Parametric Recovery of Line-of-Sight Velocity Distributions from Absorption-Line Spectra of Galaxies via Penalized Likelihood, *PASP*, 116, 138-147, 2004.
- Chilingarian I. V., Prugniel P., Sil'Chenko O. K., Afanasiev V. L., Kinematics and stellar populations of the dwarf elliptical galaxy IC 36532007, *MNRAS*, 376, 1033-1046, 2007.

- Cid Fernandes, R., González Delgado, Rosa M., Testing spectral models for stellar populations with star clusters - I. Methodology, *MNRAS*, 403, 780-796, 2010.
- Cid Fernandes, R., Mateus, A., Sodré, L., Stasínska, G., Gomes, J. M., Semi-empirical analysis of Sloan Digital Sky Survey galaxies - I. Spectral synthesis method, *MNRAS*, 358, 363-378, 2005.
- Cid Fernandes, R. & Terlevich, R., The origin of the blue continuum in type 2 Seyferts: reflection or star-forming tori, *MNRAS*, 272, 423-441, 1995.
- Colina, L., Garcia Vargas, M. L., Gonzalez Delgado, R. M., Mas-Hesse, J. M., Perez, E., Alberdi, A., Krabbe, A., On the Origin of the Ultraviolet Continuum in Seyfert 2 Galaxies, *ApJ*, 488, 71-74, 1997.
- Dimitrijević, M. S., Popović, L. Č., Kovačević, J., Dačić, M., Ilić, D., The flux ratio of the [OIII]  $\lambda\lambda 5007, 4959$  lines in AGN: comparison with theoretical calculations, *MNRAS*, 374, 1181-1184, 2007.
- Eriksson, P., Ekström, M., Melsheimer, C., Buehler, S. A. Efficient forward modelling by matrix representation of sensor responses, *International Journal of Remote Sensing*, 27, 1793-1808, 2006.
- Galavís, M. E., Mendoza C., Zeippen C.J., Atomic data from the IRON Project. XXII. Radiative rates for forbidden transitions within the ground configuration of ions in the carbon and oxygen isoelectronic sequences, *A&AS*, 123, 159-171, 1997.
- Goudfrooij P. & Emsellem E., Ionized gas in early-type galaxies: its effect on Mgb and other stellar line-strength indices, *A&A*, 306, L45-48, 1996.
- Hao, L, Strauss, M. A, Fan, X. H, Tremonti, C. A, Schlegel, D. J, et al., Active Galactic Nuclei in the Sloan Digital Sky Survey. I. Sample Selection, *AJ*, 129, 1783-1794, 2005.
- Ho, L. C, Filippenko, A. V, Sargent, W. L. W., A Reevaluation of the Excitation Mechanism of LINERs, *ApJ*, 417, 63-81, 1993.
- Keel, W. C., An H-alpha forbidden N II survey of the nuclei of a complete sample of spiral galaxies, *ApJS*, 52, 229-239, 1983.

- Kelson, D. D., Illingworth, G. D., Dokkum, P. G., Franx, M., The Evolution of Early-Type Galaxies in Distant Clusters. I. Surface Photometry and Structural Parameters for 53 Galaxies in the  $z=0.33$  Cluster CL 1358+62, *ApJ*, 531, 137-158, 2000.
- Kinney, A. L., Antonucci, R. R. J., Ward, M. J., Wilson, A. S., Whittle, M., The featureless continua and hydrogen lines of Seyfert 2 galaxies, *ApJ*, 377, 100-114, 1991.
- Koleva, M., Bouchard, A., Prugniel, P., de Rijcke, S., Vauglin, I., The transmutation of dwarf galaxies: stellar populations, *MNRAS*, 428, 2949-2965, 2013.
- Koleva, M., Prugniel, P., de Rijcke, S., Zeilinger, W. W., Age and metallicity gradients in early-type galaxies: a dwarf-to-giant sequence, *MNRAS*, 417, 1643-1671, 2011.
- Koleva, M., Prugniel, P., Bouchard, A., Wu, Y., ULYSS: a full spectrum fitting package, *A&A*, 501, 1269-1279, 2009.
- Koleva, M., Prugniel, P., Ocvirk, P., Le Borgne, D., Soubiran, C., Spectroscopic ages and metallicities of stellar populations: validation of full spectrum fitting, *MNRAS*, 385, 1998-2010, 2008.
- Koski A. T., Spectrophotometry of Seyfert 2 galaxies and narrow-line radio galaxies, *ApJ*, 223, 56-71, 1978.
- Lawson, C. L. & Hanson, R. J., Solving Least Squares Problems, *Classics in Applied Mathematics No. 15* (Philadelphia, Penn.: SIAM), 1995.
- Le Borgne D., Rocca-Volmerange B., Prugniel P., Lancon A., Fioc M., Soubiran C., Evolutionary synthesis of galaxies at high spectral resolution with the code PEGASE-HR. Metallicity and age tracers, *A&A*, 425, 881-897, 2004.
- MacArthur, L. A., González, J. J., & Courteau, S., Stellar population and kinematic profiles in spiral bulges and discs: population synthesis of integrated spectra, *MNRAS*, 395, 28-63, 2009.
- Marquart, D. W., An algorithm for least-squares estimation of nonlinear parameters, *SIAM*, 11, 431-441, 1963.
- Moore S. A. W., Lucey J. R., Kuntschner H., Colless M., Stellar populations in early-type Coma cluster galaxies - I. The data, *MNRAS*, 336, 382-408, 2002.

- Moultaka J., A new inverse method for stellar population synthesis and error analysis, *A&A*, 430, 95-106, 2005.
- Nelson, C. H. & Whittle, M., Featureless Continua and Stellar Absorption Lines in the Nuclear Spectra of Seyfert Galaxies, 197th AAS Meeting, 110.10, *Bulletin of the American Astronomical Society*, 32, 1590, 2000.
- Popović, L. Č., Smirnova, A. A., Kovačević, J., Moiseev, A. V., Afanasiev, V. L., Three-Dimensional Spectroscopic Study of the Line-Emitting Regions of Mrk 493, *AJ*, 137, 3548-3557, 2009.
- Rix, H.-W., & White, S. D. M., Optimal estimates of line-of-sight velocity distributions from absorption line spectra of galaxies - Nuclear discs in elliptical galaxies, *MNRAS*, 254, 389-403, 1992.
- Rosa, M., A Possible Nonlinearity in IDS / Image Dissector Scanner / Data, *The Messenger* 39, 15-17, 1985.
- Sarzi, M., Falcón-Barroso, J., Davies, R. L., Bacon, R., Bureau, M., Cappellari, M. et al., The SAURON project - V. Integral-field emission-line kinematics of 48 elliptical and lenticular galaxies, *MNRAS*, 366, 1151-1200, 2006.
- Sarzi, M, Rix, H-W, Shields, J. C, Ho, L. C, Barth, A. J, et al., The Stellar Populations in the Central Parsecs of Galactic Bulges, *ApJ*, 628, 169-186, 2005.
- Schmitt, H.R., Storchi-Bergmann, T., Cid-Fernandes, R., Spectral synthesis of the nuclear regions of Seyfert 2 and radio galaxies, *MNRAS*, 303, 173-178, 1999.
- Smirnova, A. A., Gavrilović, N., Moiseev, A. V., Popović, L. Č., Afanasiev, V. L., Jovanović, P.; Dačić, M., The gas kinematics in the Mrk 533 nucleus and circumnuclear region: a gaseous outflow, *MNRAS*, 377, 480-490, 2007.
- Storchi-Bergmann, T., Rainmann D., Bica E., Fraquelli H. A., The Frequency of Nuclear Star Formation in Seyfert 2 Galaxies, *ApJ*, 544, 747-762, 2000.
- Storchi-Bergmann T, Baldwin J. A, Wilson A. S., Double-peaked broad line emission from the LINER nucleus of NGC 1097, *ApJ*, 410, 11-14, 1993.
- Vanden Berk, D. E., Shen, J., Yip, C.-W., Schneider, D. P., Connolly, A. J., Burton, R. E., Jester, S., Hall, P. B., Szalay, A. S., & Brinkmann, J., Spectral Decomposition of Broad-Line AGNs and Host Galaxies, *AJ*, 131, 84-99, 2006.

- van der Marel, R. P., Velocity Profiles of Galaxies with Claimed Black-Holes - Part Three - Observations and Models for M87, MNRAS, 270, 271-297, 1994.
- Vazdekis, A., Sánchez-Blázquez, P., Falcón-Barroso, J., Cenarro, A. J., Beasley, M. A., Cardiel, N., Gorgas, J., Peletier, R. F., Evolutionary stellar population synthesis with MILES - I. The base models and a new line index system, MNRAS, 404, 1639-1671, 2010.
- Winkler, H., Glass, I. S., van Wyk, F., Marang, F., Jones, J. H. S., Buckley, D. A. H., Sekiguchi, K., Variability studies of Seyfert galaxies. I - Broad-band optical photometry, MNRAS, 257, 659-676, 1992.
- Wu, Y., Singh, H. P., Prugniel, P., Gupta, R., Koleva, M., Coudé-feed stellar spectral library - atmospheric parameters, A&A, 525, 71-92, 2011.



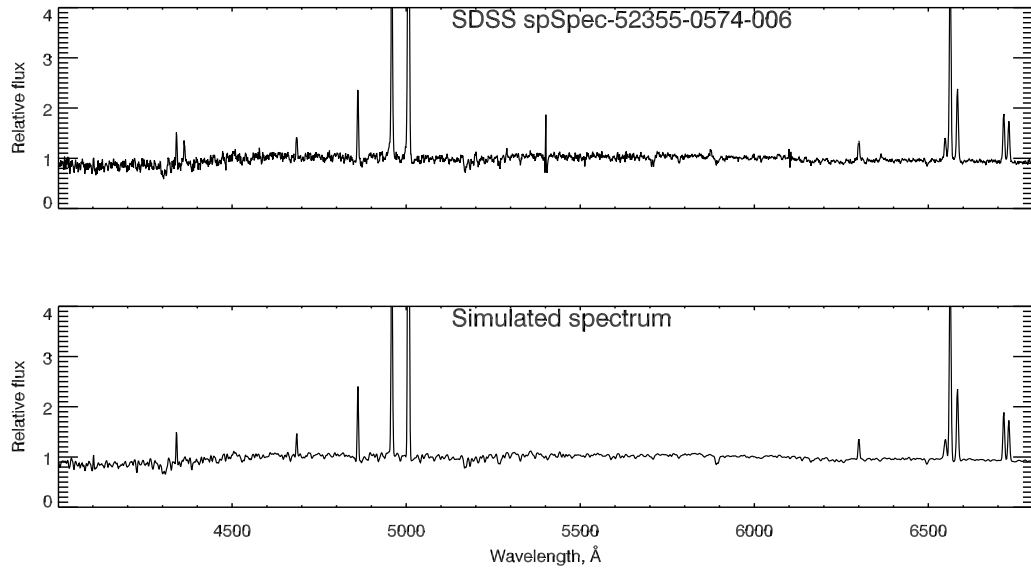
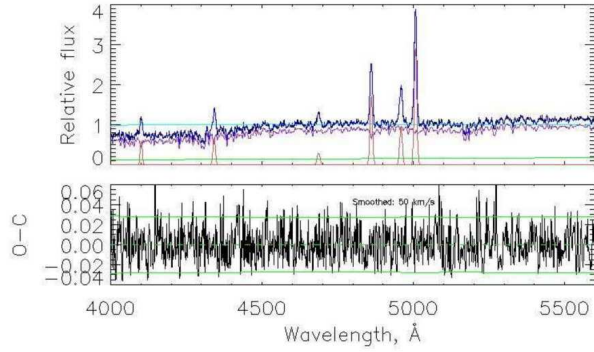


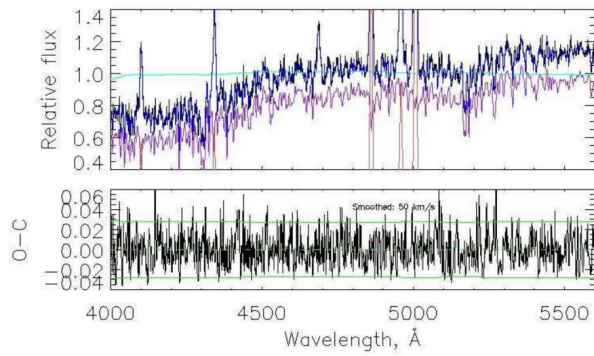
Figure 1: Comparison between real Sy2 spectrum of SDS S galaxy spSpec-52355-0574-006 (upper plot) and simulated one (bottom plot).

## 8. Figures

(a)



(b)



(c)

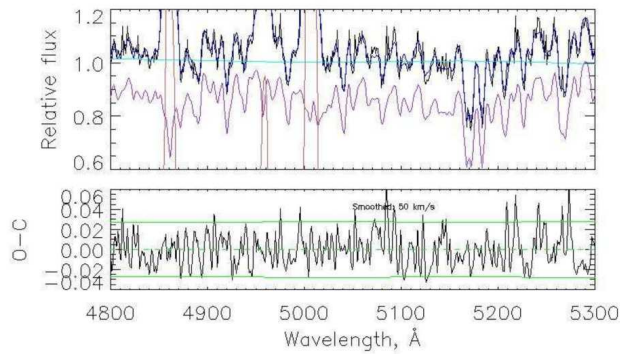


Figure 2: Panel (a) shows the fit of simulated spectra with  $\alpha=1.5$ , 10% of the AGN contribution, intensity of [OIII]4959 equal to 1, width of  $10 \text{ \AA}$ , and  $\text{SNR}=20$ . The represented wavelength range is  $\lambda\lambda = [4000 - 5600] \text{ \AA}$ . In the upper graph the black line represents the input spectrum, the blue line represents the best fit model, and the cyan line the multiplicative polynomial, while the green, light red, and violet lines represent components of the best fit model: violet – stellar population, red– emission lines, and green – AGN continuum. The bottom graph represents residuals from the best fit (black line). The green solid line shows the level of the noise, and the dashed line is the zero-axis. In order to inspect better the fit, panels (b) and (c) expand a smaller range of relative flux intensity, and smaller wavelength range, respectively.

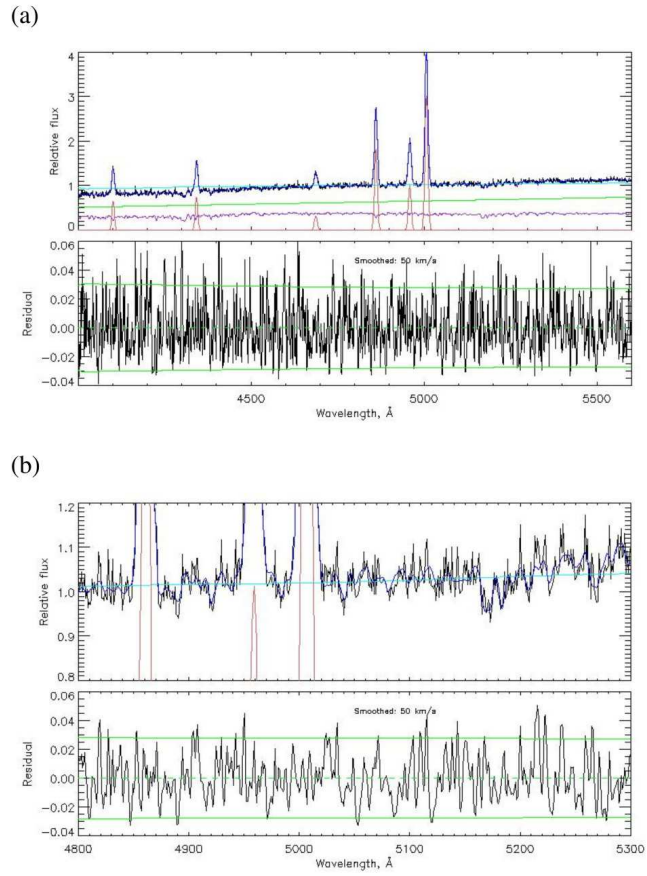
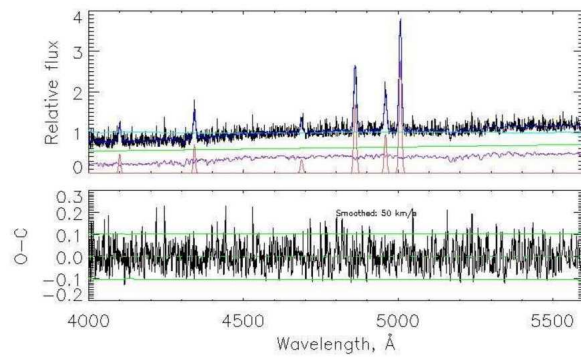


Figure 3: The panel (a) is the same as in the Fig. 2, but for 70% of AGN contribution to the total flux. The panel (b) represents the wavelength range between 4800 and 5300 Å.

(a)



(b)

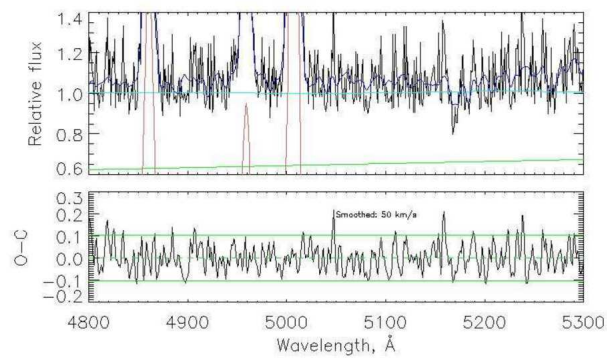


Figure 4: Fit of the simulated spectra with 50% of the AGN contribution and SNR=5. The notation is the same as in the Fig. 2

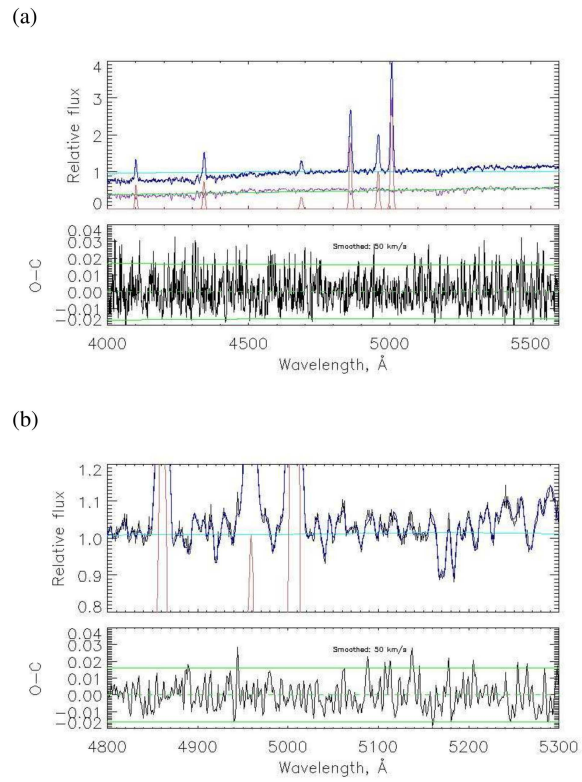


Figure 5: Fit of the simulated spectra with 50% of the FC contribution and SNR=35. The notation is the same as in the Fig.2

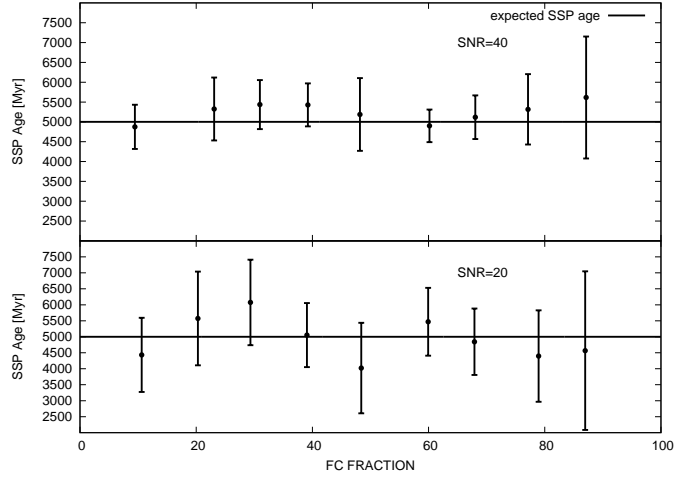


Figure 6: The restored SSP ages from the single best fit for different FC contributions to the total spectrum (10%-90%) in the cases of SNR=40 (top panel) and SNR=20 (bottom panel).

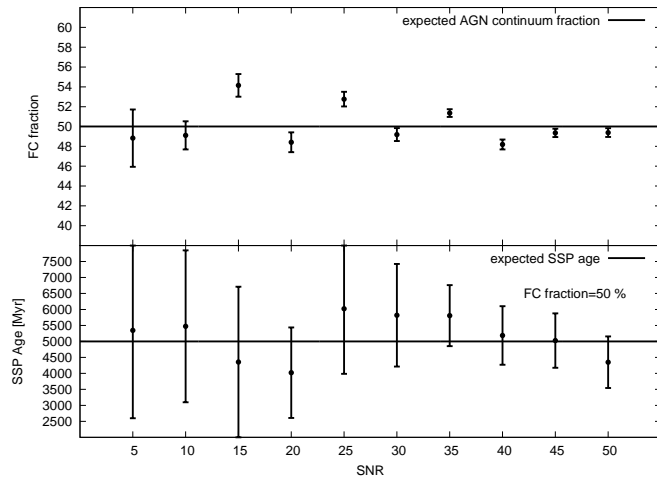


Figure 7: The restored AGN continuum fraction (top panel) and SSP age (bottom panel) from the single best fit for different signal-to-noise ratio (SNR=5-50) in the case of AGN continuum contribution of 50%.

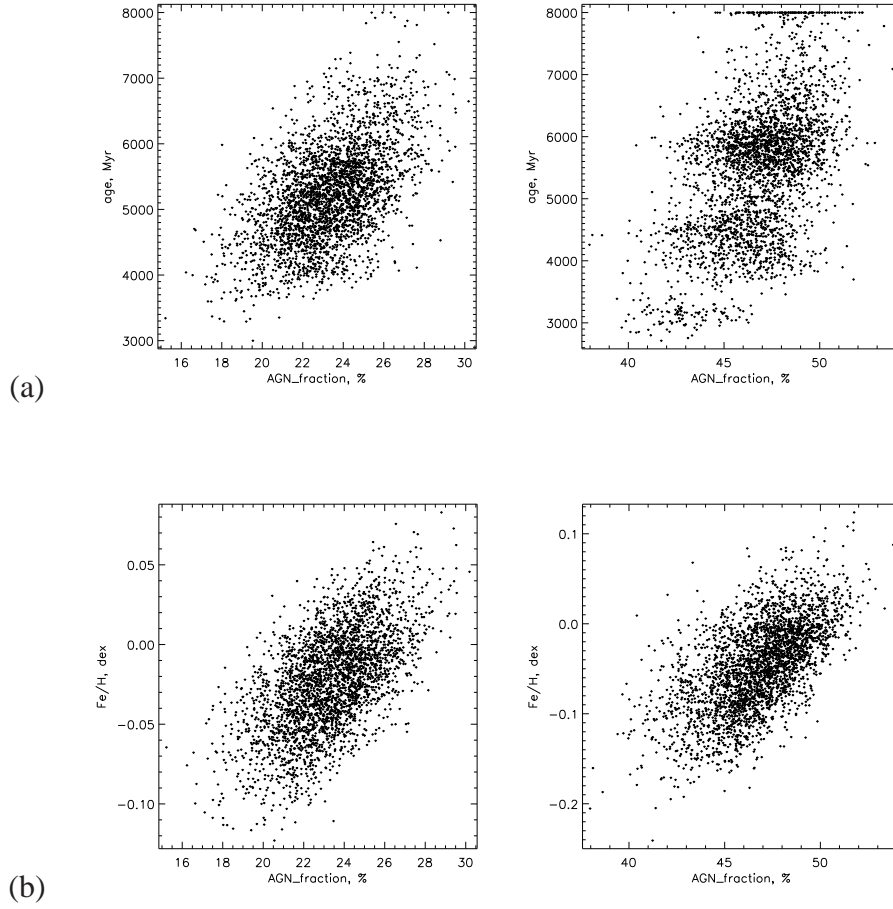


Figure 8: Result of the 3000 Monte Carlo simulations for the case of 75% (left) and 50% (right panels) of the stellar population contribution to the continuum. Plots represent dependencies between the AGN continuum contribution and (a) the metallicity of the dominated stellar population (b) mean stellar population age.

Table 1: Table lists initial values of parameters in the model and obtained results from the single best fit in the cases of different AGN continuum contributions to the total spectrum (10%-90%) and a SNR=20. Initial values in the simulation were: spectral index=1.5,  $I([\text{OIII}]4959 \text{ \AA})=1$  and  $\text{FWHM}([\text{OIII}]4959 \text{ \AA})=600 \text{ km s}^{-1}$ . Analysed spectral range was 4000-5600  $\text{\AA}$ . The variables in the table are:  $v$ -mean stellar velocity,  $\sigma_{SP}$ - stellar velocity dispersion, age of the stellar population,  $[\text{Fe}/\text{H}]$  - stellar population metallicity,  $\alpha$ -spectral index of the featureless continuum,  $f_{AGNcont}$ -restored fraction of the AGN continuum,  $f_{SP}$ -restored fraction of the SP, and  $\sigma$ -dispersion of  $\text{H}\delta$ ,  $\text{H}\gamma$ ,  $\text{HeII } 4689 \text{ \AA}$ ,  $\text{H}\beta$ ,  $[\text{OIII}]4959 \text{ \AA}$  and  $[\text{OIII}]5007 \text{ \AA}$  emission lines, respectively.

	<i>expected</i>	10% AGN	20% AGN	30% AGN	40% AGN	50%AGN	60% AGN	70% AGN	80% AGN	90% AGN
$v \text{ (km s}^{-1}\text{)}$	0	$-0.54 \pm 3.36$	$-3.09 \pm 3.95$	$-2.08 \pm 4.13$	$4.49 \pm 4.76$	$0.41 \pm 6.09$	$-11.54 \pm 6.74$	$-9.18 \pm 8.60$	$-6.84 \pm 11.03$	$6.54 \pm 15.47$
$\sigma_{SP} \text{ (km s}^{-1}\text{)}$	100	$99.84 \pm 3.72$	$101.40 \pm 4.47$	$97.10 \pm 4.67$	$96.58 \pm 5.47$	$104.30 \pm 6.93$	$88.81 \pm 7.76$	$90.69 \pm 10.06$	$74.41 \pm 13.45$	$67.30 \pm 21.49$
Age (Myr)	5000	$4433 \pm 1160$	$5573 \pm 1466$	$6075 \pm 1337$	$5052 \pm 1002$	$4021 \pm 1415$	$5470 \pm 1060$	$4844 \pm 1039$	$4397 \pm 1430$	$4566 \pm 2481$
$[\text{Fe}/\text{H}] \text{ (dex)}$	0	$-0.03 \pm 0.06$	$-0.13 \pm 0.08$	$-0.10 \pm 0.09$	$-0.06 \pm 0.11$	$0.03 \pm 0.09$	$-0.09 \pm 0.16$	$-0.07 \pm 0.22$	$-0.12 \pm 0.35$	$-0.20 \pm 0.64$
$\alpha$	1.5	$1.88 \pm 0.47$	$1.41 \pm 0.27$	$1.65 \pm 0.25$	$1.49 \pm 0.19$	$1.57 \pm 0.30$	$1.60 \pm 0.10$	$1.54 \pm 0.09$	$1.54 \pm 0.08$	$1.64 \pm 0.12$
$f_{AGNcont}$		$10.62 \pm 0.75$	$20.30 \pm 1.00$	$29.34 \pm 1.04$	$39.07 \pm 1.0$	$48.41 \pm 1.00$	$59.93 \pm 1.03$	$67.90 \pm 1.02$	$78.94 \pm 1.10$	$86.95 \pm 1.20$
$f_{SP}$		$84.50 \pm 0.73$	$74.85 \pm 0.97$	$65.83 \pm 1.02$	$56.09 \pm 0.97$	$46.76 \pm 0.98$	$35.26 \pm 1.01$	$27.25 \pm 1.01$	$16.29 \pm 1.08$	$5.87\text{e-}05 \pm 8.4\text{e-}06$
$\sigma(\text{H}\delta)$	3.48	$3.18 \pm 0.00$	$3.20 \pm 0.00$	$3.22 \pm 0.00$	$3.23 \pm 0.00$	$3.19 \pm 0.00$	$3.25 \pm 0.00$	$3.26 \pm 0.00$	$3.33 \pm 0.00$	$3.38 \pm 0.00$
$\sigma(\text{H}\gamma)$	3.68	$3.37 \pm 0.00$	$3.39 \pm 0.00$	$3.40 \pm 0.00$	$3.40 \pm 0.00$	$3.38 \pm 0.00$	$3.45 \pm 0.16$	$3.46 \pm 0.00$	$3.53 \pm 0.00$	$3.57 \pm 0.00$
$\sigma(\text{HeII } 4689 \text{ \AA})$	4.78	$4.53 \pm 0.42$	$4.56 \pm 0.43$	$4.55 \pm 0.42$	$4.38 \pm 0.43$	$4.70 \pm 0.41$	$4.87 \pm 0.40$	$4.66 \pm 0.45$	$4.79 \pm 0.44$	$4.16 \pm 0.38$
$\sigma(\text{H}\beta)$	4.13	$3.77 \pm 0.04$	$3.79 \pm 0.05$	$3.81 \pm 0.05$	$3.80 \pm 0.05$	$3.78 \pm 0.06$	$3.86 \pm 0.06$	$3.87 \pm 0.07$	$3.95 \pm 0.08$	$4.00 \pm 0.11$
$\sigma([\text{OIII}]4959 \text{ \AA})$	4.21	$3.85 \pm 0.00$	$3.87 \pm 0.00$	$3.89 \pm 0.00$	$3.89 \pm 0.00$	$3.86 \pm 0.00$	$3.94 \pm 0.00$	$3.95 \pm 0.00$	$4.03 \pm 0.00$	$4.08 \pm 0.00$
$\sigma([\text{OIII}]5007 \text{ \AA})$	4.25	$3.89 \pm 0.00$	$3.90 \pm 0.00$	$3.93 \pm 0.00$	$3.93 \pm 0.00$	$3.89 \pm 0.00$	$3.98 \pm 0.00$	$3.99 \pm 0.00$	$4.07 \pm 0.00$	$4.12 \pm 0.00$



Table 2: The same as in the Table 1, but for SNR=40.

	<i>expected</i>	10% AGN	20% AGN	30% AGN	40% AGN	50%AGN	60% AGN	70% AGN	80% AGN	90% AGN
$v$ (km s <sup>-1</sup> )	0	0.43 ± 1.69	-0.57 ± 1.87	0.23 ± 2.13	-0.38 ± 2.46	0.13 ± 2.74	-3.41 ± 3.22	-5.92 ± 4.72	-8.28 ± 6.01	0.45 ± 7.74
$\sigma_{SP}$ (km s <sup>-1</sup> )	100	100.79 ± 1.89	99.99 ± 2.10	100.4 ± 2.44	98.89 ± 2.83	91.97 ± 3.09	85.94 ± 3.71	83.23 ±	92.77 ± 7.20	74.77 ± 10.64
Age (Myr)	5000	4875 ± 558	5325 ± 794	5436 ± 618	5428 ± 542	5187 ± 916	4900 ± 410	5118 ± 550	5316 ± 887	5615 ± 1538
[Fe/H] (dex)	0	-0.03 ± 0.03	0.04 ± 0.04	0.01 ± 0.04	-0.04 ± 0.05	-0.06 ± 0.05	0.00 ± 0.08	-0.09 ± 0.11	-0.08 ± 0.17	0.00 ± 0.3
$\alpha$	1.5	1.28 ± 0.37	1.49 ± 0.15	1.42 ± 0.11	1.46 ± 0.09	1.51 ± 0.15	1.55 ± 0.40	1.57 ± 0.04	1.57 ± 0.03	1.63 ± 0.04
$f_{AGN,cont}$		9.45 ± 0.45	23.10 ± 0.45	30.96 ± 0.42	39.23 ± 0.48	48.19 ± 0.50	60.16 ± 0.49	68.04 ± 0.53	77.12 ± 0.52	87.12 ± 0.47
$f_{SP}$		85.57 ± 0.44	71.95 ± 0.43	64.12 ± 0.41	55.85 ± 0.47	46.91 ± 0.49	34.92 ± 0.47	27.04 ± 0.52	18.00 ± 0.51	7.61e-05 ± 4.39e-06
$\sigma(H\delta)$	3.48	3.20 ± 0.00	3.20 ± 0.00	3.20 ± 0.00	3.20 ± 0.00	3.24 ± 0.00	3.29 ± 0.00	3.29 ± 0.00	3.23 ± 0.00	3.33 ± 0.00
$\sigma(H\gamma)$	3.68	3.39 ± 0.00	3.39 ± 0.00	3.38 ± 0.00	3.39 ± 0.00	3.43 ± 0.00	3.48 ± 0.16	3.49 ± 0.00	3.42 ± 0.00	3.52 ± 0.00
$\sigma(\text{HeII } 4689 \text{ \AA})$	4.78	4.56 ± 0.21	4.84 ± 0.23	4.60 ± 0.22	4.52 ± 0.22	4.41 ± 0.20	4.62 ± 0.22	4.49 ± 0.22	4.67 ± 0.22	4.80 ± 0.22
$\sigma(H\beta)$	4.13	3.79 ± 0.02	3.79 ± 0.02	3.80 ± 0.02	3.79 ± 0.03	3.84 ± 0.03	3.90 ± 0.03	3.90 ± 0.03	3.82 ± 0.05	3.94 ± 0.06
$\sigma([\text{OIII}]\lambda 4959 \text{ \AA})$	4.21	3.87 ± 0.00	3.87 ± 0.00	3.86 ± 0.00	3.87 ± 0.00	3.91 ± 0.00	3.98 ± 0.00	3.98 ± 0.00	3.90 ± 0.00	4.02 ± 0.00
$\sigma([\text{OIII}]\lambda 5007 \text{ \AA})$	4.25	3.91 ± 0.00	3.91 ± 0.00	3.90 ± 0.00	3.91 ± 0.00	3.95 ± 0.00	4.01 ± 0.00	4.02 ± 0.00	3.94 ± 0.00	4.06 ± 0.00

Table 3: The same as in the Table 1, but for 50% of AGN continuum contribution and for signal-to-noise ratios between 5 and 50.

	<i>expected</i>	SNR=5	SNR=10	SNR=15	SNR=20	SNR=25	SNR=30	SNR=35	SNR=40	SNR=45	SNR=50
$v$ (km s <sup>-1</sup> )	0	-8.56 ± 13.56	-6.80 ± 9.54	-3.16 ± 7.04	0.41 ± 6.09	-2.11 ± 4.57	-1.43 ± 3.68	-1.74 ± 2.53	0.13 ± 2.74	-2.43 ± 2.53	-2.10 ± 2.56
$\sigma_{SP}$ (km s <sup>-1</sup> )	100	82.05 ± 17.63	94.45 ± 10.94	92.69 ± 8.15	104.30 ± 6.93	91.76 ± 5.18	92.30 ± 4.16	95.09 ± 2.88	91.97 ± 3.09	100.54 ± 2.96	96.02 ± 2.84
Age (Myr)	5000	5345 ± 2749	5473 ± 2375	4356 ± 2356	4021 ± 1415	6023 ± 2036	5819 ± 1606	5807 ± 954	5187 ± 916	5026 ± 852	5349 ± 807
[Fe/H] (dex)	0	0.10 ± 0.35	0.16 ± 0.19	0.08 ± 0.12	0.03 ± 0.09	0.00 ± 0.08	-0.06 ± 0.07	0.04 ± 0.04	-0.06 ± 0.03	-0.03 ± 0.05	0.03 ± 0.04
$\alpha$	1.5	1.51 ± 0.39	1.37 ± 0.20	1.42 ± 0.44	1.57 ± 0.30	1.57 ± 0.26	1.53 ± 0.22	1.48 ± 0.09	1.51 ± 0.15	1.37 ± 0.30	1.54 ± 0.22
$f_{AGNcont}$	50	48.83 ± 2.89	49.11 ± 1.42	54.15 ± 1.14	48.41 ± 1.00	52.76 ± 0.74	49.19 ± 0.65	51.36 ± 0.39	48.19 ± 0.50	49.36 ± 0.42	49.39 ± 0.44
$f_{SP}$		46.89 ± 2.83	46.32 ± 1.39	41.13 ± 1.11	46.74 ± 0.98	42.38 ± 0.72	45.95 ± 0.63	43.73 ± 0.38	46.91 ± 0.49	45.73 ± 0.41	45.67 ± 0.43
$\sigma(H\delta)$	3.48	3.21 ± 0.00	3.21 ± 0.00	3.27 ± 0.00	3.19 ± 0.00	3.23 ± 0.00	3.24 ± 0.00	3.22 ± 0.00	3.24 ± 0.00	3.19 ± 0.00	3.23 ± 0.00
$\sigma(H\gamma)$	3.68	3.40 ± 0.00	3.40 ± 0.00	3.46 ± 0.00	3.38 ± 0.00	3.42 ± 0.00	3.43 ± 0.16	3.41 ± 0.00	3.43 ± 0.00	3.38 ± 0.00	3.42 ± 0.00
$\sigma(\text{HeII } 4689 \text{ \AA})$	4.78	4.32 ± 1.56	3.96 ± 0.69	5.18 ± 0.60	4.70 ± 0.41	4.78 ± 0.32	4.43 ± 0.27	4.53 ± 0.18	4.41 ± 0.20	4.54 ± 0.18	4.60 ± 0.18
$\sigma(H\beta)$	4.13	3.81 ± 0.17	3.81 ± 0.10	3.87 ± 0.07	3.78 ± 0.06	3.83 ± 0.04	3.84 ± 0.03	3.81 ± 0.02	3.84 ± 0.03	3.78 ± 0.03	3.83 ± 0.02
$\sigma([\text{OIII}]4959 \text{ \AA})$	4.21	3.89 ± 0.00	3.89 ± 0.00	3.95 ± 0.00	3.86 ± 0.00	3.91 ± 0.00	3.91 ± 0.00	3.89 ± 0.00	3.91 ± 0.00	3.86 ± 0.00	3.91 ± 0.00
$\sigma([\text{OIII}]5007 \text{ \AA})$	4.25	3.92 ± 0.00	3.92 ± 0.00	3.99 ± 0.00	3.89 ± 0.00	3.95 ± 0.00	3.95 ± 0.00	3.93 ± 0.00	3.95 ± 0.00	3.90 ± 0.00	3.95 ± 0.00

Table 4: The same as in the Table 1, but for 50% of AGN continuum contribution, SNR=20 and spectral range  $\lambda\lambda = [4000 - 6700]\text{\AA}$ .

	<i>expected</i>	<i>obtained</i>
$v$ (km s <sup>-1</sup> )	0	-6.54 ± 5.72
$\sigma_{SP}$ (km s <sup>-1</sup> )	100	92.55 ± 6.53
Age (Myr)	5000	5517 ± 1596
[Fe/H] (dex)	0	0.07 ± 0.09
$\alpha$	1.5	1.64 ± 0.28
$f_{AGN_{cont}}$	50	53.04 ± 0.94
$f_{SP}$		40.76 ± 0.92
$\sigma(\text{H}\delta)$	3.48	3.24 ± 0.00
$\sigma(\text{H}\gamma)$	3.68	3.42 ± 0.00
$\sigma(\text{HeII } 4689 \text{ \AA})$	4.78	5.06 ± 0.51
$\sigma(\text{H}\beta)$	4.13	3.83 ± 0.06
$\sigma([\text{OIII}]4959 \text{ \AA})$	4.21	3.88 ± 0.00
$\sigma([\text{OIII}]5007 \text{ \AA})$	4.25	3.95 ± 0.00
$\sigma([\text{NII}]6548 \text{ \AA})$	5.56	5.21 ± 0.00
$\sigma(\text{H}\alpha)$	5.57	5.17 ± 0.00
$\sigma([\text{NII}]6583 \text{ \AA})$	5.59	5.24 ± 0.00

Table 5: The same as in the Table 4, but for spectral range  $\lambda\lambda = [4000 - 5600]\text{\AA}$ .

	<i>expected</i>	<i>obtained</i>
$v$ (km s <sup>-1</sup> )	0	0.41 ± 6.09
$\sigma_{SP}$ (km s <sup>-1</sup> )	100	104.30 ± 6.93
Age (Myr)	5000	4020 ± 1415
[Fe/H] (dex)	0	0.03 ± 0.09
$\alpha$	1.5	1.57 ± 0.30
$f_{AGN_{cont}}$	50	48.41 ± 1.00
$f_{SP}$		46.74 ± 0.98
$\sigma(\text{H}\delta)$	3.48	3.19 ± 0.00
$\sigma(\text{H}\gamma)$	3.68	3.38 ± 0.00
$\sigma(\text{HeII } 4689 \text{ \AA})$	4.78	4.70 ± 0.41
$\sigma(\text{H}\beta)$	4.13	3.78 ± 0.06
$\sigma([\text{OIII}]4959 \text{ \AA})$	4.21	3.86 ± 0.00
$\sigma([\text{OIII}]5007 \text{ \AA})$	4.25	3.89 ± 0.00

Table 6: The same as in the Table 4, but for spectral range  $\lambda\lambda = [4200 - 5600]\text{\AA}$ .

	<i>expected</i>	<i>obtained</i>
$v$ (km s <sup>-1</sup> )	0	-2.91 ± 6.33
$\sigma_{SP}$ (km s <sup>-1</sup> )	100	97.07 ± 7.34
Age (Myr)	5000	4628 ± 1117
[Fe/H] (dex)	0	0.02 ± 0.12
$\alpha$	1.5	1.63 ± 0.52
$f_{AGN_{cont}}$	50	49.75 ± 1.25
$f_{SP}$		45.32 ± 1.24
$\sigma(\text{H}\gamma)$	3.68	3.38 ± 0.00
$\sigma(\text{HeII } 4689 \text{ \AA})$	4.78	4.40 ± 0.42
$\sigma(\text{H}\beta)$	4.13	3.79 ± 0.06
$\sigma([\text{OIII}]4959 \text{ \AA})$	4.21	3.86 ± 0.00
$\sigma([\text{OIII}]5007 \text{ \AA})$	4.25	3.90 ± 0.00